Title

Stress-activated pyrolytic carbon nanofibers for electrochemical platforms

Authors

Holmberg, Sunshine
Ghazinejad, Maziar
Cho, EunByul
et al.

Publication Date

2018-11-01

DOI

10.1016/j.electacta.2018.09.013

Electrochimica Acta 290 (2018) 639–648

Contents lists available at ScienceDirect

Electrochimica Acta

journal homepage: www.elsevier.com/locate/electacta

Stress-activated pyrolytic carbon nanofibers for electrochemical platforms

Sunshine Holmberg [a, 1], Maziar Ghazinejad [b, *, 1], EunByul Cho [c], Derosh George [a], Brandon Pollack [a], Alexandra Perebikovsky [d], Regina Ragan [e], Marc Madou [a, **]

[a] Department of Mechanical and Aerospace Engineering, University of California, Irvine, CA, 92697, USA
[b] Department of Mechanical and Aerospace Engineering, University of California, San Diego, CA, 92093, USA
[c] Department of Biomedical Engineering, University of California, Irvine, CA, 92697, USA
[d] Department of Physics and Astronomy, University of California, Irvine, CA, 92697, USA
[e] Department of Chemical Engineering and Materials Science, University of California, Irvine, CA, 92697, USA

ARTICLE INFO

Article history:
Received 29 May 2018
Received in revised form
29 August 2018
Accepted 3 September 2018
Available online 14 September 2018

Keywords:
Pyrolytic carbon
Electrochemical sensing
Carbon microstructure
Electrocatalysis

ABSTRACT

Carbon's electrochemistry depends on its type and microstructure, and how these affect the electrode's electronic density of states. We demonstrate how pyrolysis of electro-mechanically stressed Polyacrylonitrile (PAN) nanofibers, infused with carbon nanotubes, will result in a unique graphitic electrode, which possesses enhanced and multifaceted electrochemical behavior. As corroborated by materials characterization, the microstructure of the stress-activated pyrolytic carbon (SAPC) characteristically contains a high proportion of disorders in the forms of edge planes and embedded heterogeneous nitrogen atoms. These disorders introduce a range of energy states near the Fermi level, yielding enhanced kinetics in the as-synthesized SAPC electrodes. A comprehensive electrochemical study of the SAPC electrode in surface sensitive ($[Fe(CN)_6]^{3-/4-}$), surface insensitive ($[IrCl_6]^{2-/3-}$), and adsorption sensitive (dopamine) redox probes demonstrates 5–14-fold increases in its heterogeneous electron transfer rate compared to regular PAN-based carbon electrodes. The fast kinetics of SAPC electrodes in adsorption sensitive analytes translates into its capability for simultaneous detection of dopamine, uric acid, and ascorbic acid. The results point to a new class of pyrolytic carbon electrodes with an attractive electrocatalytic capacity, geared toward electrochemical sensing platforms.

1. Introduction

In recent years, carbon has gained growing interest as a material of choice for a variety of technological applications ranging from energy storage devices, such as proton exchange membrane (PEM) fuel cells, to chemical and biological sensors, such as glucose and pH sensors [1–7]. Carbon's attractive electronic and structural properties, and superb electrochemical stability, make it especially suited for contemporary electrochemical applications. The challenge in using carbon as an electrode material is to fabricate inexpensive carbon electrodes with an enduring electrocatalytic performance [8–10]. This challenge largely stems from carbon's unique and variable electronic density of states (DOS) [10,11]. Since a higher DOS increases the probability of electron transfer between an electrode and redox system, a low DOS near the fermi level generally translates to sluggish electrochemical kinetics. For instance, crystalline graphitic materials, while possessing prized electronic and mechanical characteristics, are largely made up of organized basal planes with low electronic DOS near the Fermi level, giving them subpar electrochemical performance. This phenomenon is also common in glassy carbon (GC), which is far more disorganized than graphite, but shares a similar electronic structure around the Fermi energy [10,12–15].

Since electrochemistry is largely an interfacial phenomenon, a common strategy to enhance carbon's electrochemical kinetics is to modify its surface by a variety of activation techniques, including polishing, heat treatment, laser irradiation and electrochemical pretreatment [10,16–18]. The core of this strategy is to generate surface and structural defects that introduce new electronic states

* Corresponding author.
** Corresponding author.
E-mail addresses: mghazinejad@ucsd.edu (M. Ghazinejad), mmadou@uci.edu (M. Madou).
[1] These authors contributed equally.

https://doi.org/10.1016/j.electacta.2018.09.013
0013-4686/

at energy levels around the E° of the redox systems of interest. Consequently, these defects will function as favorable sites for electron transfer. Another approach to improve carbon electrochemistry is to employ nanocarbon allotropes, namely graphene and CNTs. While these nanocarbons characteristically exhibit better electrochemical behavior, they are expensive to synthesize and their electrochemical behavior depends mainly on their graphitic edge planes. Therefore, fabrication of efficient electrodes from these nanocarbons involves processing steps to increase the ratio of edge to basal planes, or to insert heteroatoms into their graphitic crystal lattice. Heteroatoms, such as nitrogen, act as electron donors, creating carbon with n-type conductivity and improved electrochemical performance. While these modifications effectively boost carbon's electrochemical performance, they require additional, complex post-processing steps and are inherently transient in nature [19,20].

Here, we report on a pyrolytic carbon with high electrocatalytic activity, stemming from its graphitized structure that is inherently rich in nitrogen heteroatoms and edge planes. To develop this pyrolytic carbon, a polyacrylonitrile (PAN) polymer precursor, naturally rich in nitrogen, is pyrolyzed at low-temperatures to retain target heteroatoms in its carbon microstructure. Furthermore, PAN's graphitization is increased beyond its natural propensity by implementing electrohydrodynamic forces (caused by addition of MWCNTs to PAN precursors) and mechanical stresses, which align PAN molecular chains through the dielectrophoresis and confinement effect [21]. A comprehensive electrochemical and material characterization showed a correlation between the microstructure and electrocatalytic performance of the synthesized carbon. Raman spectroscopy, High Resolution Transmission Electron Microscopy (HRTEM), and X-ray Photoelectron Spectroscopy (XPS), reveal that the pyrolytic carbon has a unique graphitized microstructure, which features abundant edge planes and nitrogen heteroatoms. To understand the underlying electrochemistry of the pyrolytic carbon, SAPC's electrochemical response towards three different redox systems with varying surface and adsorption sensitivities was studied. The results demonstrate an overall enhancement in degree and stability of the pyrolytic carbon's electrochemical kinetics, with a particularly high capacity for electron transfer with adsorption sensitive species. This high electrocatalytic performance allows for simultaneous detection of multiple adsorptive species, such as dopamine, uric acid, and ascorbic acid.

The implemented synthesis approach eliminates the need for additional post-processing to functionalize carbon electrodes. Furthermore, the low-temperature pyrolysis, necessary for retention of the heteroatoms from the selected organic precursors, reduces the cost and time of carbon fabrication. The results of this study reveal a new class of pyrolytic carbon with a long-lasting, efficient electrocatalytic capacity that holds promise for electrochemical sensing and energy storage applications.

2. Materials and methods

2.1. Electrospinning

Polyacrylonitrile (PAN) (Sigma Aldrich) with a molecular weight of 150,000 g/mol, *N*,N-dimethylformamide (DMF) (Sigma Aldrich) and multi-walled carbon nanotubes (MWCNT) (Sigma Aldrich) were used to obtain pure PAN mats and PAN-CNT mats via electrospinning. To obtain a solution with a final concentration of 8% PAN for electrospinning, PAN powder was dissolved in DMF. The mixture of PAN and DMF was stirred for 24 h at 40° C to ensure homogeneity. Solution for preparing PAN-CNT mats was obtained by dispersing MWCNT into DMF by ultrasonicating the mixture for 1 h. This mixture was then stirred for 24 h to avoid agglomeration of MWCNT. PAN was then added to the mixture and stirred for another 24 h to obtain a final solution containing 1% MWCNT and 8% PAN.

The pure PAN and PAN-CNT mats were electrospun by applying a potential of 1.6 kV between a continuously dispensing syringe (0.25 mL/h) and a rotating, metallic drum collector (rotating at 500 RPM). The mats were removed from the drum after electrospinning for 4hrs.

2.2. Mechanical treatment and stabilization

Prior to stabilization, PAN-CNT mats were mechanically rolled using a Dayton roller press to further align the carbon molecular chains. These PAN-CNT mats were then compressed to 200 kPa and stabilized at 280 °C for 6 h to obtain mechanically treated PAN-CNT mats, the precursor to SAPC. Pure PAN mats underwent no mechanical treatment and were stabilized at 280 °C immediately following electrospinning.

2.3. Carbonization

The mats were pyrolyzed in an inert, nitrogen gas environment (flow rate of 9000 sccm) inside a Lindberg Blue M tube furnace. To increase graphitization and prevent nanoporosity of the carbon, a two-step pyrolysis process was used. The mats were first heated to 300 °C at a rate of 4.5 °C/min and kept at this temperature for an hour. The temperature was then increased to 1000 °C at 2.5 °C/min and held at this value for an hour before cooling down to the ambient temperature.

2.4. Electrochemical characterization

The carbon mats produced though pyrolysis were cut into smaller pieces (about 3 × 10 mm) for electrochemical characterization. Carbon electrodes were fabricated by connecting a thin copper wire to the mat using conductive carbon paste (Structure Probe, Inc.). Polydimethylsiloxane (PDMS) (Dow Corning Corporation) was used to secure the electrode onto a 15 × 20 mm glass slide, see Fig. 1. Electrochemical tests were carried out using a Princeton Applied Research VersaSTAT 4 Potentiostat.

The electroactive surface area of the sample was calculated using electrochemical impedance spectroscopy (EIS). EIS was performed in a blank electrolyte solution of 1X Phosphate Buffered Saline (PBS) at a frequency of 10,000 Hz–0.1 Hz. An equivalent circuit [22] was used to fit the resultant Nyquist plot data. The electroactive surface area was determined using equation (1)

$$A_{act} = \frac{I_c}{C_{dl}{}^{*}\nu} \tag{1}$$

where the double-layer specific capacitance, C_{dl}, was determined by normalizing the capacitance value of the equivalent circuit by that of the geometric surface area of the electrode. The scan rate (V/s), ν, and the double-layer charging current, I_c, were obtained using cyclic voltammetry (CV).

3. Results and discussion

3.1. Material synthesis and characterization

Carbon's electrochemical behavior varies considerably based on its synthesis method, microstructure, and chemistry. A number of studies suggest that graphitic edge planes and embedded heteroatoms enhance carbon electron transfer due to a higher electronic DOS at these “defects” [10,11,23,24]. Accordingly, a significant

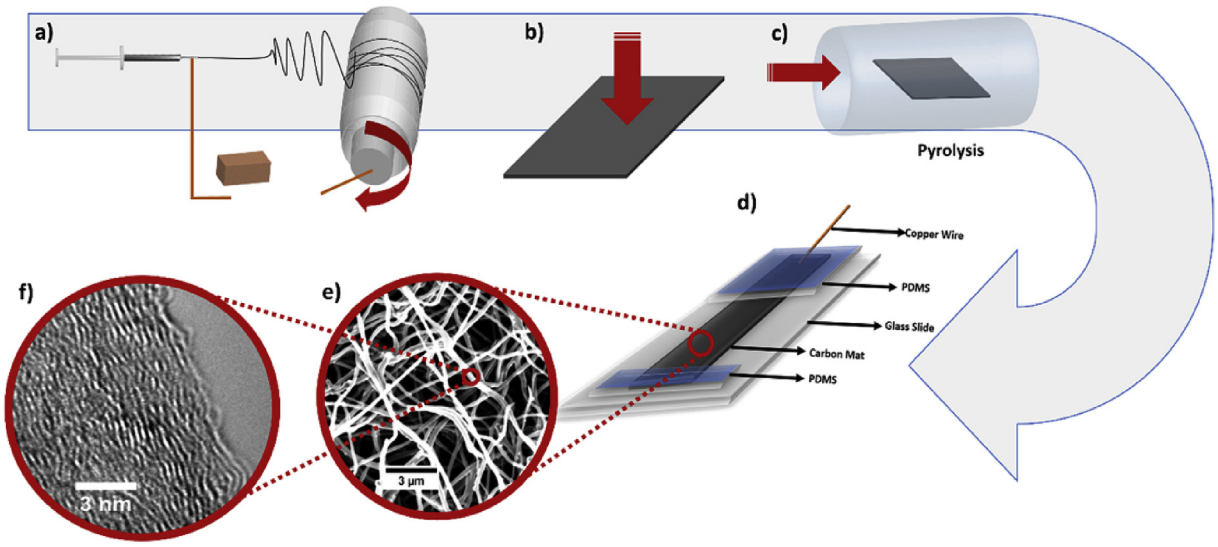

Fig. 1. Schematic diagram of the SAPC electrode fabrication process. a) MWCNT-infused PAN solution is electrospun onto a rotating drum. b) PAN-CNT nanofiber mat is thermally stabilized under compressive stress. c) Processed PAN-CNT nanofiber mats are pyrolyzed under nitrogen flow at 1000 °C. d) Carbonized mats are cut into rectangular electrodes and are electrically connected by attaching copper wires. e) Scanning electron micrograph of SAPC nanofibers. f) Transmission electron micrograph of SAPC nanofibers.

amount of carbon research has focused on tuning these features to improve carbon's electrochemical performance [24–26]. In our previous work, we demonstrated how inducing molecular alignment in organic precursors can influence their carbonization upon pyrolysis [21]. Based on this method, we introduced a polyacrylonitrile (PAN)-based pyrolytic carbon with a uniformly graphitized structure, which is inherently abundant in edge planes. Additionally, the proposed synthesis method uses low-temperature pyrolysis, which retains PAN's nitrogen atoms within the resulting carbon structure. Therefore, we anticipate that the unique structure of this pyrolytic carbon, and its propensity for incorporating nitrogen heteroatoms, will result in a boosted electrochemical response.

Following the procedure outlined in our previous work, we use electrohydrodynamic forces to orient the PAN molecular chains within the electrospun polymer fibers [21]. The polymer was subsequently stabilized under a compressive stress (to maintain the alignment of the precursor's chains) and pyrolyzed at 1000 °C (Fig. 1). Detailed characterization of the resulting carbon was then conducted to investigate the correlation between its electrochemical behavior and microstructure. High Resolution Transmission Electron Microscopy (HRTEM) allowed us to visually study the correlation between the synthesis method and the carbon's microstructure. Fig. 2a and b demonstrate the microstructures of untreated PAN-based pyrolytic carbon nanofibers (PNF) and stress activated PAN-based carbon nanofibers (SAPC), respectively.

A quick examination of the HRTEM micrographs reveals a remarkable improvement in ordering of pyrolytic carbon when it is produced from stress-aligned polymer chains. As can be seen in Fig. 2bi, the mechanically treated carbon displays relatively aligned carbon planes with wavy fringes. By contrast, the micrograph of PNF in Fig. 2ai shows far less distinctive features with more circular, cage-like microstructures commonly seen in amorphous or glass-like carbons [27,28]. Additionally, the oriented, but short and wavy fringes of SAPC display a graphitized structure with a high quantity of edge planes. The abundance of these “disorders” is associated with higher electronic DOS near the Fermi level, which translate into enhanced electrochemical transfer kinetics.

Raman Spectroscopy allows for quantifying the degree and uniformity of graphitization of the material. Averaged Raman spectra and Raman maps were determined based on 100 spectra collected across 5 µm × 5 µm areas of the PNF mats (Fig. 2 aii and 2 bii). The quality of graphitization can be evaluated by the ratio of the D peak intensity, centered between 1300 and 1400 cm^{-1}, to that of the G peak, located between 1560 and 1600 cm^{-1}. The G peak is related to the in-plane bond stretching motion of pairs of sp^2-hybridized carbon atoms and the D peak is related to the disorder and deviation from perfect graphitic structure [29]. Hence, the lower the D to G ratio (I_D/I_G), the higher the level of graphitization within the carbon. Lorentzian curve fitting [30] was employed to decompose the Raman spectra to its constituent peaks, including D and G peaks. Analysis of the resolved Raman peaks suggest a substantial enhancement in the graphitization of PAN-based carbon after stress-induced molecular alignment, with the average I_D/I_G dropping from 1.47 to 0.90. Furthermore, this enhancement in graphitization of SAPC electrodes is prevalent throughout the nanofibers mats, as corroborated by the uniform Raman mapping of the resulting carbon. This uniform graphitization also translates to notably higher conductivity in PAN-based carbon fabrics [21].

We also performed Raman and Energy Dispersive X-ray spectroscopies on the applied MWCNT to ensure their structural and compositional quality (Figs. S3 and S4c in supplementary information). The results demonstrate the high graphitic quality and purity of the used MWCNTs. This observation is particularly important, as the presence of metallic residues in the embedded MWCNTs could influence the electrochemical characterization of SAPC, thus making it difficult to establish structure-property relationships for SAPC electrodes.

To investigate the presence of heterogeneous atoms and the composition of the PAN-based carbons, we employed X-ray Photoelectron Spectroscopy (XPS). The XPS data reveals the presence of nitrogen and oxygen in the pyrolytic carbon, with a composition breakdown of 94.5 ± 0.1 at.% carbon, 4.4 ± 0.5 at.% nitrogen and 1 ± 0.3 at.% oxygen (Fig. 2c and d). Using Lorentzian curve fitting to deconvolute the nitrogen peak, N 1s, a rather unique distribution of nitrogen groups is found, comprised of 19.2% pyridinic, 57.0% graphitic, and a negligible amount of pyrrolic nitrogen atoms in the synthesized carbon fibers [19,31,32]. The detected nitrogen heteroatoms originate from the nitrogen-rich PAN precursors that endured the low-temperature pyrolysis. The

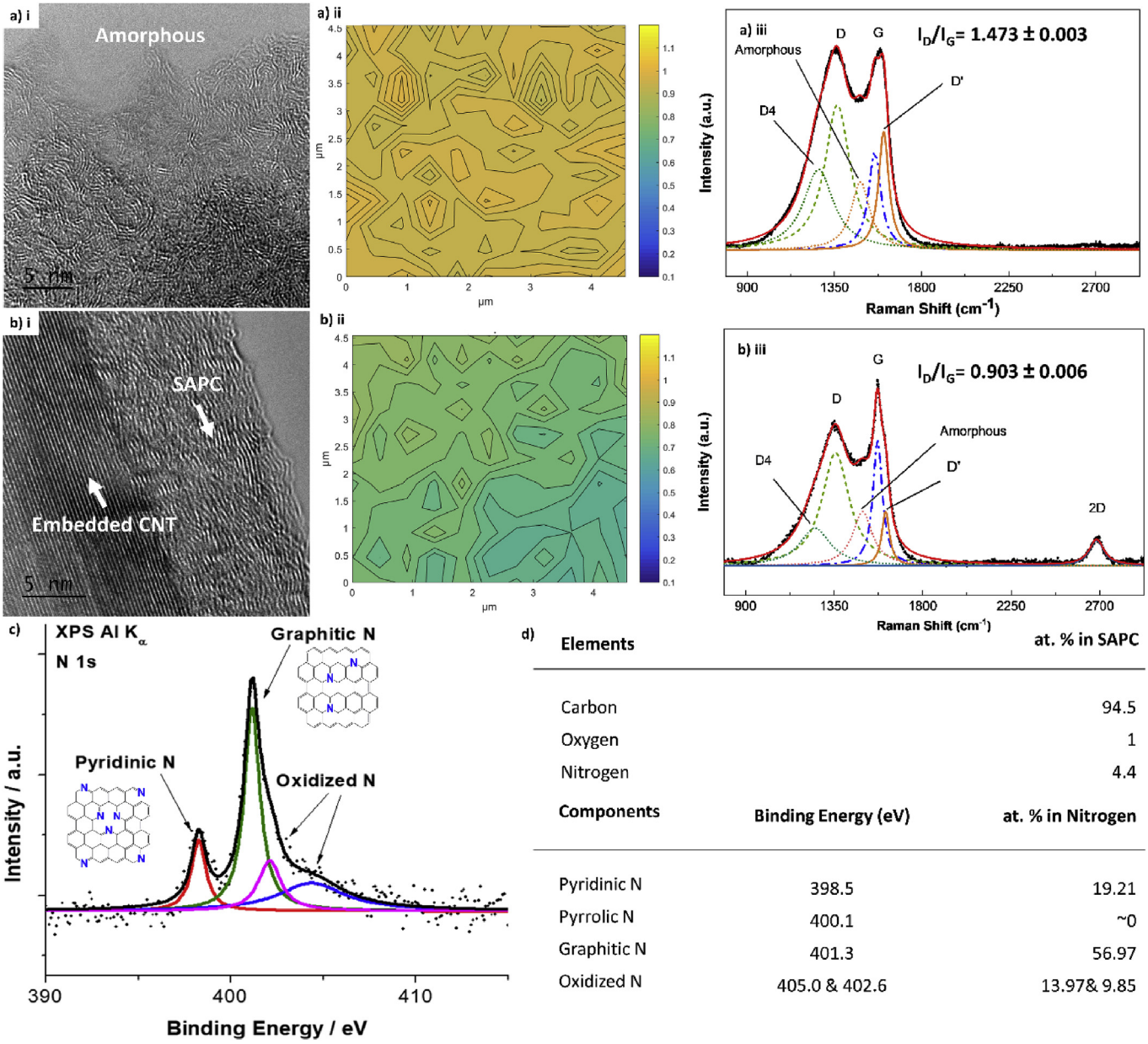

Elements		at. % in SAPC
Carbon		94.5
Oxygen		1
Nitrogen		4.4
Components	**Binding Energy (eV)**	**at. % in Nitrogen**
Pyridinic N	398.5	19.21
Pyrrolic N	400.1	~0
Graphitic N	401.3	56.97
Oxidized N	405.0 & 402.6	13.97& 9.85

Fig. 2. Material characterization of SAPC and untreated PAN-based PNF. High Resolution Transmission Electron Microscopy (HRTEM) of: ai) PNF and bi) SAPC microstructures. Mapping of Raman spectroscopy I_D/I_G ratio of: aii) PNF, and bii) SAPC. Average Raman spectrum of aiii) PNF and biii) SAPC electrodes. Averages of over 100 collections are used to represent PNF and SAPC ($\lambda_{excitation} = 532$ nm). (c) XPS spectrum of the N 1s peak of SAPC. (d) Table of elemental composition of the SAPC as determined by analysis of XPS spectrum.

breakdown of the nitrogen heteroatoms in the synthesized carbon is of particular interest for its electrochemical performance [19,20]. It is important to note that the nitrogen heteroatoms are inherent in the as-pyrolyzed carbon, and no additional post-synthesis process, such as doping, has to be applied.

3.2. Electrochemical characterization

The presence of disorders in carbon electrodes increases the electronic states with energy levels that overlap with the E° of the redox system, thus enhancing electron transfer rates. For electrodes tested in outer-sphere redox systems (surface sensitive analytes), the disorders in the underlying microstructure of the carbon affect the electronic DOS. In the case of inner sphere redox systems (surface insensitive analytes), the electronic DOS and electron transfer rate depend on the carbon surface defects and their interactions with the redox systems.

Accordingly, to probe our new carbon material for different electrochemical behaviors, we study its electrochemical response in three different redox systems: potassium hexachloroiridate $[IrCl_6]^{2-/3-}$ (surface insensitive), potassium ferricyanide $[Fe(CN)_6]^{3-/4-}$ (surface sensitive), and dopamine (adsorption surface sensitive) [10,11,26]. Cyclic voltammograms in these solutions allowed us to investigate the electrochemical kinetics of four different electrode materials (PNF, SAPC, polished Glassy Carbon, and MWCNT) by determining the heterogeneous electron transfer rate (k^o_{app}), the ratio between the reduction and oxidation current peaks (I_{red}/I_{ox}), and the linearity between the current peaks and the square root of the scan rate. Figs. 3 and 4 summarize the results.

The k^o_{app} values shown in the electrochemical kinetics table in

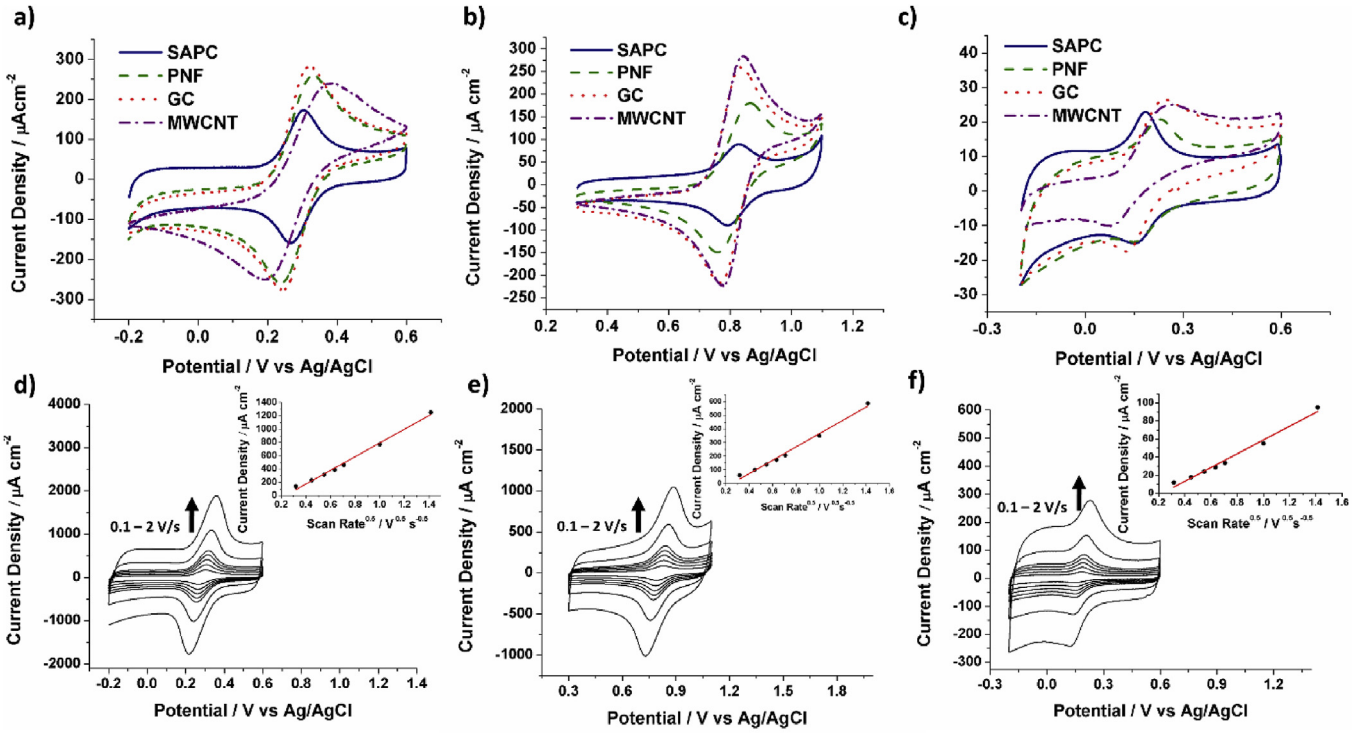

Fig. 3. Electrochemical kinetics of SAPC. Cyclic voltammograms of SAPC, PNF, GC and MWCNT's electrochemical response to aqueous solution of: a) 2 M KCl and 1 mM of $K_3Fe(CN)_6$, b) 2 M KCl and 1 mM of K_3IrCl_6, and c) pH 7.4, 1 mM PBS at and 0.1 mM of dopamine at a scan rate of 100 mV/s. Electrochemical response of SAPC to varying scan rates in aqueous solutions of d) 2 M KCl and 1 mM of $K_3Fe(CN)_6$, e) 2 M KCl and 1 mM of K_3IrCl_6 and f) pH 7.4, 1 mM PBS at and 0.1 mM of Dopamine.

Fig. 4d are determined using the Nicholson method, which assumes the behavior of the carbon electrodes is comparable to that of 2D planar electrodes. The validity of this assumption is seen in the collected voltammograms in Fig. 3, which demonstrate a linear relation between the square root of the scan rate and the peak current density [11,33]. To study the three different carbon electrodes systematically, we first analyze their electrochemical behavior within each aqueous redox probe, and then compare their varying performances across the different probes.

As mentioned earlier, potassium $[IrCl_6]^{2-/3-}$ is an outer-sphere redox probe. Due to the tunneling of electrons through the electrode surface, the response of carbon electrodes in $[IrCl_6]^{2-/3-}$ is more susceptible to the underlying carbon microstructure and is insensitive to the defects and interactions occurring on the surface [10,11]. Thus, potassium $[IrCl_6]^{2-/3-}$ is a suitable electrochemical probe for structural analysis of our pyrolytic carbon fibers. As seen in Fig. 4d, SAPC exhibits an electron transfer rate (k^o_{app}) that is nearly 8 times greater than that of PNF (0.0461 cm s^{-1} vs. 0.00586 cm s^{-1}), and nearly two times greater than that of alumina-polished glassy carbon (0.0461 cm s^{-1} vs. 0.0232 cm s^{-1}), a standard activated carbon electrode used here as a control. The enhanced kinetics of SAPC in $[IrCl_6]^{2-/3-}$ underlines the high proportion of disorders in the form of edge sites within the structure of the SAPC electrodes. As predicted for surface insensitive analytes, microstructural defects do more to improve electrochemical kinetics than simple mechanical roughening of the electrode surface.

To investigate the effects of surface interactions and defects on the three pyrolytic carbons, we use $[Fe(CN)_6]^{3-/4-}$, a benchmark inner-sphere redox probe with high kinetic sensitivity to the state of electrode surfaces [10,11,34]. Here, the electron transport kinetics show a similar upward trend, with SAPC electrodes exhibiting k^o_{app} values 14 times greater than PNF electrodes (0.114 cm s^{-1} vs. 0.00795 cms^{-1}) and 10 times greater than alumina-polished glassy carbons (0.114 cm s^{-1} vs. 0.0135 cms^{-1}). The higher k^o_{app} values determined in $[Fe(CN)_6]^{3-/4-}$ (compared to that of $[IrCl_6]^{2-/3-}$) points to the effectiveness of our carbon synthesis method in boosting surface features of SAPC, i.e., edge planes and other electroactive sites. Indeed, HRTEM characterization of the carbon electrode surface corroborates this electrochemical deduction (Figs. 2-bi and 4a) [21]. The improved surface kinetics of SAPC over that of mechanically roughened glassy carbon is due to the stable and persistent nature of the energy states in the surface sites of SAPC. The coarse nature of the mechanical abrasion used to polish glassy carbon electrodes produces defects that are electrochemically unstable and transient [25,35]. On the other hand, the surface states of SAPC electrodes are forged at the elevated temperatures of the pyrolysis process and are therefore more resistant to passivation. This phenomenon is discussed further in the stability analysis of the electrodes.

Perhaps, the most interesting electrochemical responses is obtained in dopamine redox system, whose complex electrocatalytic interaction with carbon electrodes offers a variety of insights. Dopamine is an inner-sphere analyte that is principally sensitive to adsorption and the state of electrode surface [10,36], and mostly indifferent to their inner structure. In this context, a dramatic shift in behavior is observed between the carbon electrodes; for the first time, the k^o_{app} of the amorphous PNF is higher than that of the more structured GC. Furthermore, the electrochemical kinetics of SAPC with dopamine marks the largest enhancement from polished glassy carbon (0.0418 cm s^{-1} vs. 0.0146 cms^{-1}), pointing to adsorption mechanisms that are active on the surface of PAN based electrodes. Additionally, the ratio between the reduction and oxidation current (I_{red}/I_{ox}) is near unity for SAPC, much higher than for PNF and GC (0.751 and 0.705, respectively). This discrepancy can be explained by looking a little closer at the complexity of Dopamine electrochemistry.

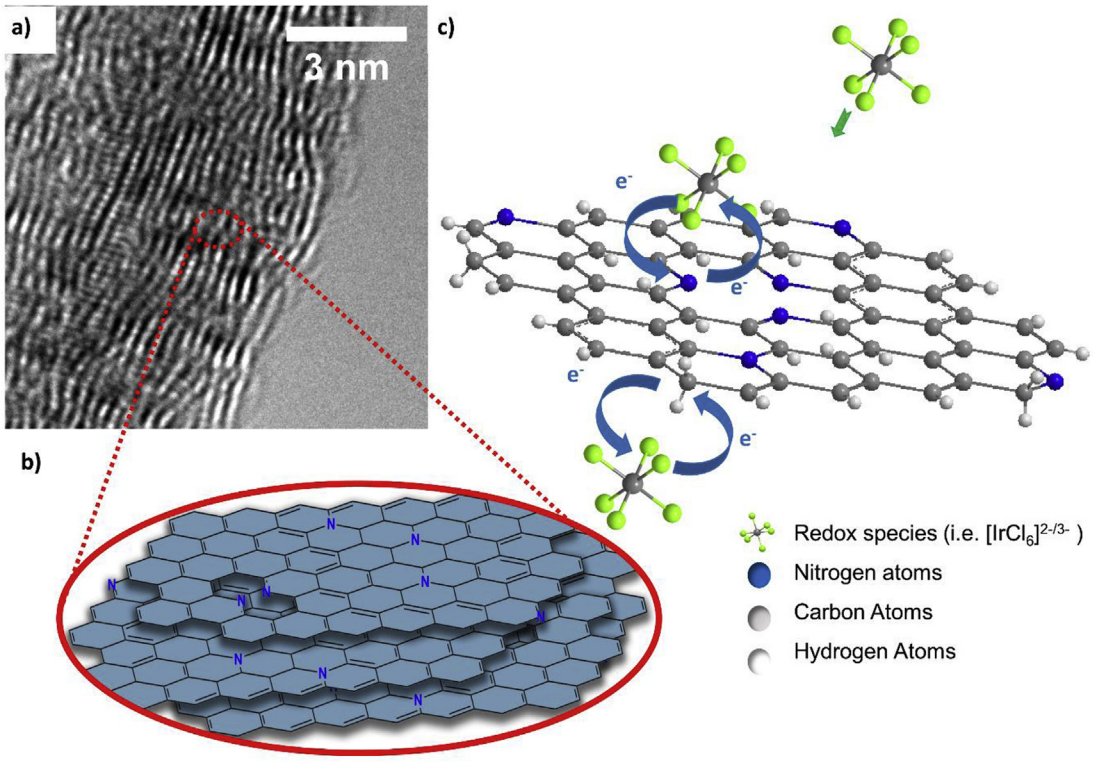

d)

Carbon Type	PNF	SAPC	Alumina-Polished Glassy Carbon	MWCNT*
[Fe(CN)$_6$]$^{3-/4-}$				
k^o_{app} (cm/s)	0.00795	0.114	0.0135	0.00121
I_{red}/I_{ox}	0.99	0.99	0.99	0.97
[IrCl$_6$]$^{2-/3-}$				
k^o_{app} (cm/s)	0.00586	0.0461	0.0232	0.0103
I_{red}/I_{ox}	0.99	0.99	0.99	0.99
Dopamine				
k^o_{app} (cm/s)	0.00861	0.0418	0.00146	0.00133
I_{red}/I_{ox}	0.751	0.92	0.705	0.781

Fig. 4. Enhanced quantity of electroactive sites on SAPC electrode due to its characteristic microstructure and composition. (a) HRTEM imaging of SAPC suggests a high ratio of edge to basal planes within its microstructure. (b) Depiction of graphitic and pyridinic nitrogen heteroatoms in SAPC lattice. (c) Enhanced heterogeneous electron transfer at electroactive nitrogen heteroatoms and carbon edge sites in SAPC electrodes. (d) Electrochemical kinetics values of SAPC, PNF, Alumina-Polished glassy carbon and MWCNT in different redox systems. *The measured k^o_{app} represents the electrochemical response of the MWCNT used in synthesis of SAPC.

The electrooxidized form of Dopamine (Dopamine o-quinone) can undergo chemical oxidation, which reduces its concentration by converting it to an electrochemically inert agent [37,38]. An observed drop in the reduction peak of dopamine reflects this phenomenon. However, it is believed that adsorption due to π-π stacking and interactions between hydrogen groups at edge planes can favor Dopamine o-quinone's electrochemical reduction over its chemical oxidation, thus improving its kinetics [32,39,40]. For carbon electrodes, adsorption sites are mostly located near graphitic edge planes where heteroatoms are present and provide the necessary dipole interaction for adsorption to occur. This is supported by the results of XPS analysis that revealed a significant quantity of nitrogen heteroatoms on the surface of the PAN-based electrodes. Though XPS data shows the presence of oxygen groups as well, prior studies have shown that oxygen concentrations below 7% have negligible effects on the kinetics of dopamine electro-oxidation [41]. Therefore, the enhanced kinetics of dopamine are likely caused by the electrocatalytic performance of the electrodes' nitrogen groups or graphitic edge planes. Overall, the electrochemical performance displayed by the SAPC is comparable to some of the highest performing carbon electrodes studied to date, including reduced-graphene oxide and laser-activated GC electrodes [10,42,43]. Fig. 4b and c visualize the discussed mechanisms contributing to the enhanced electrochemical kinetics of SAPC electrodes in different redox probes systems.

To investigate the possible influence of embedded MWCNT on the electrochemical response of SAPC electrodes, we carried out a set of cyclic voltammetry on pure MWCNT electrodes, fabricated by standard drop casting method (Fig. 3a–c, and 4d). As it can be seen from Fig. 3a–c and table in Fig. 4d, the electrochemical performance of pure MWCNTs electrodes is significantly subpar compared to that of SAPC electrodes, with $k^o_{app,\ SAPC}$ 5 to 94 times larger than $k^o_{app,\ MWCNT}$ in different redox probes. The vast difference between electrochemical responses of MWCNT and SAPC

electrodes indicates the independence of SAPC electrochemical performance from that of MWCNT. This observation is also consistent with the fact that MWCNT are abundant in basal planes and scarce in electrochemically favored edge planes and heteroatoms. The superiority SAPC electrodes over MWCNT electrodes is particularly evident in surface sensitive species, namely Potassium Ferricyanide and Dopamine.

Another important aspect of carbon electrodes' performance is their electrochemical stability. It is anticipated that the robust, single-step fabrication process for SAPC's will result in a high electrochemical stability for their electrodes. Additionally, compared to other nitrogen-doped carbons, SAPC has a rather unique composition of C-N groups, consisting of primarily graphitic and pyridinic nitrogen atoms at a ratio of 3:1. Both these nitrogen groups are highly stable [19,32,44,45]. To evaluate the stability of SAPC's electrochemical response, cyclic voltammetry was performed with each redox system on SAPC electrodes for 300 cycles at 100 mV/s (~1.5 h per test). The results of the stability characterization are shown in Fig. S1 are extensively discussed in the supplementary documents of this report. The 3-day tests reveal the SAPC electrodes to be far more stable that than the industry-standard activated HOPG and GC electrodes, and comparable to expensive graphene-based electrodes in all three redox probe systems. Please see the supplementary documents and Fig. S1 for further discussion on the stability characterization of SAPC.

3.3. Simultaneous electrocatalytic detection of dopamine, uric acid, and ascorbic acid

The good electrocatalytic behavior of SAPC in adsorption-sensitive analytes makes this carbon electrode an appealing candidate for biosensing applications. A particular area of interest in biochemical sensing is the simultaneous electrochemical detection of ascorbic acid (AA), uric acid (UA) and dopamine (DA). AA, UA, and DA are important biomarkers whose concentration within the body can be directly attributed to health status of the host [32,40,46,47]. Shifts in the concentration levels of AA, UA, and DA have been directly linked to neurodegenerative diseases such as Parkinson's and Alzheimer's, prompting research into the development of simple, sensitive, and selective biosensors.

Carbon electrodes traditionally have subpar performance for simultaneous detection of AA, UA, and DA because the electrochemical responses for these analytes generally overlaps [46,47]. As illustrated in the cyclic voltammograms in Fig. 5, the degree of separation between the peak potentials of AA, UA, and DA directly correlates with the heterogenous electron rates, determined in the earlier sections. For carbons lacking an adequate quantity of strong adsorption sites (such as glassy carbon) the sluggish electron transfer kinetics results in a drastic positive shift in oxidation peak potential for all three species, causing their response to overlap and become indiscernible. As the surface of carbon is modified to enhance the adsorption and electron transfer kinetics of the three species, the individual oxidation peaks of each species undergo a negative potential shift, differentiating them from each other (Fig. 5) [32,40,47].

SAPC's superior kinetics is evident from the appearance of the AA peak at higher scan rates (100 mV/s) during simultaneous detection (Fig. 5a). This is absent in the PNF's simultaneous response (Fig. 5b), but is present in its individual response (Fig. 5e). The disappearance of the AA peak in the simultaneous response of PNF is due to the slower kinetics, forcing competition among the three electroactive species for electron transfer at the PNF's active

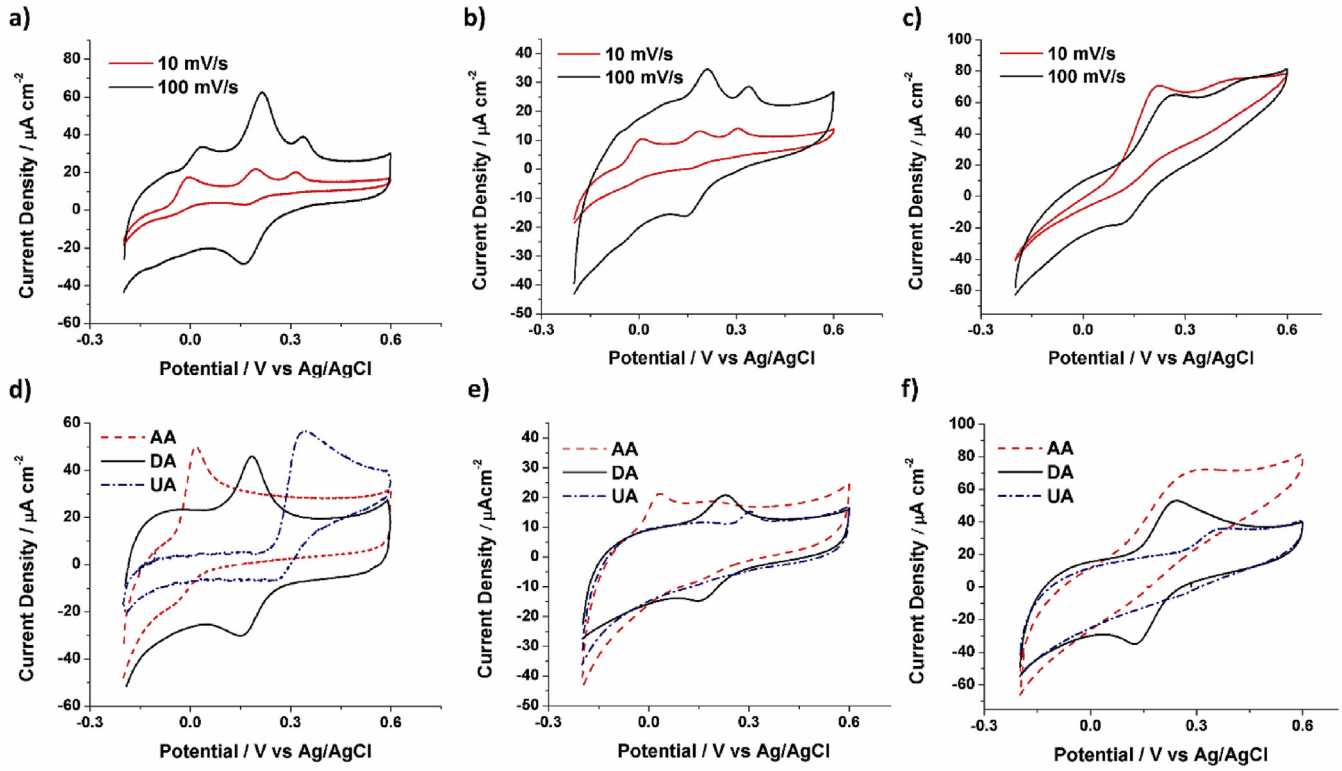

Fig. 5. Electrocatalytic oxidation of dopamine, ascorbic acid and uric acid. Cyclic voltammograms of a) SAPC, b) PNF and c) GC electrodes' response to in 1 mM ascorbic acid, 0.1 mM uric acid and 0.1 mM dopamine in a pH 7.4 PBS buffer. Combined cyclic voltammograms of d) SAPC, e) PNF and f) GC electrodes' responses to separate solutions of in 1 mM ascorbic acid in pH 7.4 PBS buffer, 0.1 mM uric acid in pH 7.4 PBS buffer and 0.1 mM dopamine in a pH 7.4 PBS buffer.

sites. This effect becomes noticeably worse at higher concentrations of UA (1 mM), DA (1 mM) and AA (10 mM), since the charge transfer and transport begins to saturate. The SAPC's superior electrocatalysis for adsorption sensitive species is further demonstrated here, as its voltammogram continues to exhibit three distinct peaks, even at these higher concentrations (Fig. S2). For both concentrations, SAPCs simultaneous response shows the peaks of AA, DA, and UA to be located between -2.76 mV and 37 mV, 198 mV and 214 mV, and 316 mV and 337 mV, respectively. This separation in electrochemical response results in an average difference of 189 mV between the AA and DA peaks (ΔE_{DA-AA}), and 120 mV between the DA and UA peaks (ΔE_{UA-DA}). Furthermore, these peak separations are comparable to those seen in prior studies on graphene-based electrodes [32,40,47]. The distinguishable electrochemical response and lack of interference between the electroactive species makes SAPC a superior platform for simultaneous detection of these bioanalytes.

To further investigate the SAPC's ability for simultaneous detection of AA, UA, and DA, Differential Pulse Voltammetry (DPV) was used. DPV is a highly sensitive voltammetric sweep technique that decouples the background capacitive current from the faradaic response [48]. DPV was performed in 1 mM PBS buffer (pH 7.4) in a potential range between -0.2 and 0.6 V vs Ag/AgCl. Each test began with a PBS solution containing 50 μM AA, 5 μM DA and 5 μM UA. For this test, the concentration of the target analyte is incrementally increased while the remaining two analytes' concentrations are kept constant.

Fig. 6 demonstrates the results of the DPV test. The correlation between the current density and the bioanalytes' concentration is extracted from their respective peak current density in DPV (insets of Fig. 6). The linear correlation between the peak current density and the concentration of the analytes allows us to determine the sensitivity of the SAPC from the slope of the curve. It was determined that the SAPC electrode displays sensitivities of 0.189 μA cm^{-2} μM^{-1}, 1.51 μA cm^{-2} μM^{-1}, and 5.21 μA cm^{-2} μM^{-1} for detecting AA, UA, and DA, respectively. The limit of detection (LOD) can therefore be estimated using equation (2) [49].

$$LOD = \frac{3\sigma}{S} \quad (2)$$

where σ is the standard deviation of the current signal in a blank solution and S is the sensitivity. A signal to noise (S/N) of 3 is used for the calculation. As summarized in Fig. 6d, the calculated sensitivity and limits of detection are comparable to the highest values reported to date for graphene-based electrodes [32,40,47]. It is also important to note that the peak current density of each electroactive species is not influenced by the addition of the other two species. The linearity of calibration curves for SAPC allows us to determine the sensitivity and the LOD for DA, UA and AA analytes. The appearance of dual linear regions in the peak current of DPV as a function of the dopamine concentration can be due to the

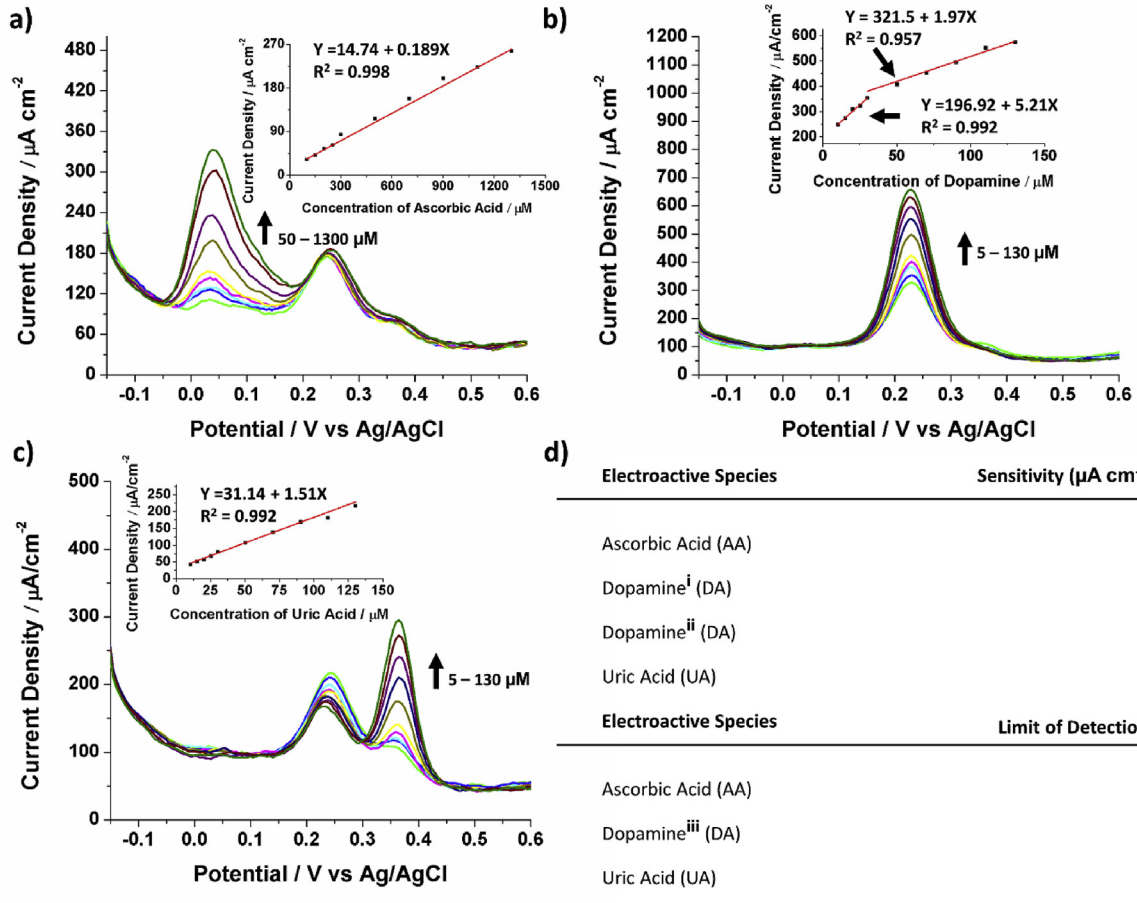

d)

Electroactive Species	Sensitivity (μA cm^{-2} μM^{-1})
Ascorbic Acid (AA)	0.189
Dopamine[i] (DA)	5.21
Dopamine[ii] (DA)	1.97
Uric Acid (UA)	1.51
Electroactive Species	**Limit of Detection (μM)**
Ascorbic Acid (AA)	3.162
Dopamine[iii] (DA)	0.114
Uric Acid (UA)	0.396

Fig. 6. Differential Pulse Voltammetry (DPV). DPV of SAPC response to aqueous pH 7.4 PBS buffer solution containing a) 50 μM AA, 5 μM DA, 5 μM UA, b) 50 μM AA, 5–130 μM DA, 5 μM UA and c) 50 μM AA, 5 μM DA, 5–130 μM UA. Insets show the relationship between peak current density and concentration. d) Table summarizing the sensitivity and limit of detection of SAPC to each analyte. SAPC's dopamine sensitivity measured by: [i] lower linear region, and [ii] higher linear region. [iii] The LOD of dopamine is determined using the sensitivity of the lower linear region.

saturation of the active sites by DA species (Fig. 6b). At high concentrations, this phenomenon is further exacerbated and its effects can be visually seen by large shifts in the current peak locations of AA, UA and DA in their respective cyclic voltammograms (Fig. 4). Consequently, the calibration curve exhibits a bilinear behavior and can be fitted with two linear regressions. Overall, the similarities among the electrochemical response of SAPC, graphene nanoflakes [47] and nitrogen-doped graphene [32,39,40] suggest that the high sensitivity and rapid kinetics of SAPC originates from a combination of its abundant edge planes and heteroatoms.

To compare the capacity of the embedded MWCNTs for simultaneous electrochemical detection of AA, UA, and dopamine, we performed a set of similar cyclic and differential pulse voltammetry on MWCNT electrodes (Fig. S5). The obtained voltammograms demonstrate that not only the signal from MWCNT is very low, but also all three species (AA, DA and UA) have overlapping peaks, inhibiting MWCNT's ability to differentiate their signals. Such overlapping is due to MWCNT's sluggish electrochemical kinetics, which results in a drastic shift in the AA peak location. The observed lack of selectivity in the carbon nanotube is consistent with the previous electrochemical characterization of MWCNT electrodes in dopamine, where SAPC outperforms MWCNT, as demonstrated by a 31-fold decrease in heterogeneous electron transfer rate of MWCNT ($k^o_{\text{app, MWCNT}} = 0.00133$) compared to that of SAPC ($k^o_{\text{app, SAPC}} = 0.0418$) (Figs. 3c and 4d). This comparative study corroborates that the enhanced electrochemical performance of SAPC stems from its unique microstructure and heteroatoms, rather than the presence of MWCNTs in it.

4. Conclusion

In this work, we investigated the correlation between the microstructure of pyrolytic carbon, its disorders, and electrochemical functionality. Using a stress-induced process, we demonstrated how realignment of PAN molecular chains produces a uniformly graphitized carbon. The resulting carbon exhibit an oriented but fragmented lattice structure, as visualized by HRTEM imaging. Further material characterization with XPS indicates that the stress activated pyrolytic carbon is innately rich in nitrogen heteroatoms.

The presence of these chemical and structural disorders in the SAPC prompted us to perform a comprehensive electrochemical study with surface insensitive (potassium hexachloroiridate), surface sensitive (potassium ferricyanide), and adsorption sensitive (dopamine) electroactive species. The electrochemical kinetics show that SAPC's heterogenous electron transfer rate is 5–14 times higher than that of standard pyrolytic PAN carbons and 2 to 10 times higher than polished commercial glassy carbon in both the surface insensitive and sensitive redox probes. The results underline the correlation between the enhanced sensitivity of SAPC towards surface sensitive species and the numerous graphitic edges and nitrogen heteroatoms present in the carbon lattice. The presence of these “defects” is associated with the quantity of the electroactive sites on the carbon electrodes.

The unique electrocatalytic behavior of SAPC allows for an efficient and simultaneous detection of dopamine (DA), ascorbic acid (AA), and uric acid (UA), without the need for post-processing of the pyrolytic carbon. The results demonstrate that SAPC has a sensitivity and limit of detection for dopamine that compares favorably with expensive graphene and CNT based sensors. The capability of SAPC for detecting biomarkers indicates its potential for biomedical sensing applications. Additionally, SAPC is mechanically more robust compared to its graphene-based counterparts.

It is important to note that the mere presence of heterogeneous atoms and edge planes in carbon structure does not constitute enhanced electrochemical behavior, since their effect could be countered by a low-degree of graphitization in the resulting carbon. The results reported here suggest that a key concept in carbon's electrochemistry is the right amount of select “disorders” within a generally “ordered” framework. The former increases the localized DOS around the E° of the redox systems of interest, facilitating heterogeneous electron transfer, and the latter enhances electron transport within the carbon electrode. The introduced stress-activation route harnesses the versatility of carbon by producing a graphitic framework, which features heteroatoms and structural disorders that are tuned for electrochemical performance.

Funding source

This work is partially funded by National Science Foundation (NSF) grant #1449397.

Acknowledgments

The authors appreciate the National Science Foundation (NSF) grant #1449397 for financial support. The authors thank UCI's Chemistry Department Laser Spectroscopy Facility and the Fuel Cell Research Center (FCRC) for the access to their facilities, equipment and materials. S.H. would also like to acknowledge Alejandro Urdaneta-Carrera for his technical assistance in performing the electrochemical characterization.

Appendix A. Supplementary data

Supplementary data related to this article can be found at https://doi.org/10.1016/j.electacta.2018.09.013.

References

[1] A.L. Dicks, The role of carbon in fuel cells, J. Power Sources 156 (2006) 128–141, https://doi.org/10.1016/j.jpowsour.2006.02.054.
[2] Z. Zhu, L. Garcia-Gancedo, A.J. Flewitt, H. Xie, F. Moussy, W.I. Milne, A critical review of glucose biosensors based on carbon nanomaterials: carbon nanotubes and graphene, Sensors 12 (2012) 5996–6022, https://doi.org/10.3390/s120505996.
[3] J. Wang, Carbon-nanotube based electrochemical biosensors: a review, Electroanalysis 17 (2005) 7–14, https://doi.org/10.1002/elan.200403113.
[4] K. Scida, P.W. Stege, G. Haby, G.A. Messina, C.D. García, Recent applications of carbon-based nanomaterials in analytical chemistry: critical review, Anal. Chim. Acta 691 (2011) 6–17, https://doi.org/10.1016/j.aca.2011.02.025.
[5] F.A. de Bruijn, V. a. T. Dam, G.J.M. Janssen, Review: durability and degradation issues of PEM fuel cell components, Fuel Cell. 8 (2008) 3–22, https://doi.org/10.1002/fuce.200700053.
[6] E. Frackowiak, F. Béguin, Carbon materials for the electrochemical storage of energy in capacitors, Carbon 39 (2001) 937–950, https://doi.org/10.1016/S0008-6223(00)00183-4.
[7] A. Singh, J. Jayaram, M. Madou, S. Akbar, Pyrolysis of negative photoresists to fabricate carbon structures for microelectromechanical systems and electrochemical applications, J. Electrochem. Soc. 149 (2002) E78–E83, https://doi.org/10.1149/1.1436085.
[8] D. Krishnan, F. Kim, J. Luo, R. Cruz-Silva, L.J. Cote, H.D. Jang, J. Huang, Energetic graphene oxide: challenges and opportunities, Nano Today 7 (2012) 137–152, https://doi.org/10.1016/j.nantod.2012.02.003.
[9] H.Y. Mao, S. Laurent, W. Chen, O. Akhavan, M. Imani, A.A. Ashkarran, M. Mahmoudi, Graphene: promises, facts, opportunities, and challenges in nanomedicine, Chem. Rev. 113 (2013) 3407–3424, https://doi.org/10.1021/cr300335p.
[10] R.L. McCreery, Advanced carbon electrode materials for molecular electrochemistry, Chem. Rev. 108 (2008) 2646–2687, https://doi.org/10.1021/cr068076m.
[11] D.A.C. Brownson, D.K. Kampouris, C.E. Banks, Graphene electrochemistry: fundamental concepts through to prominent applications, Chem. Soc. Rev. 41 (2012) 6944, https://doi.org/10.1039/c2cs35105f.
[12] M.S. Dresselhaus, G. Dresselhaus, J.E. Fischer, Graphite intercalation compounds: electronic properties in the dilute limit, Phys. Rev. B 15 (1977) 3180–3192, https://doi.org/10.1103/PhysRevB.15.3180.
[13] K.J. Koivusaari, T.T. Rantala, S. Leppävuori, Calculated electronic density of states and structural properties of tetrahedral amorphous carbon, Diam. Relat.

Mater. 9 (2000) 736–740, https://doi.org/10.1016/S0925-9635(99)00286-1.
[14] J. Robertson, E.P. O'Reilly, Electronic and atomic structure of amorphous carbon, Phys. Rev. B 35 (1987) 2946–2957, https://doi.org/10.1103/PhysRevB.35.2946.
[15] K.R. Kneten, R.L. McCreery, Effects of redox system structure on electron-transfer kinetics at ordered graphite and glassy carbon electrodes, Anal. Chem. 64 (1992) 2518–2524.
[16] R.K. Jaworski, R.L. McCreery, Laser activation of carbon microdisk electrodes: surface oxide effects on Ru (NH3) 62+ 3+ kinetics, J. Electroanal. Chem. 369 (1994) 175–181.
[17] R.J. Rice, N.M. Pontikos, R.L. McCreery, Quantitative correlations of heterogeneous electron-transfer kinetics with surface properties of glassy carbon electrodes, J. Am. Chem. Soc. 112 (1990) 4617–4622.
[18] S. Ranganathan, T.-C. Kuo, R.L. McCreery, Facile preparation of active glassy carbon electrodes with activated carbon and organic solvents, Anal. Chem. 71 (1999) 3574–3580.
[19] H. Wang, T. Maiyalagan, X. Wang, Review on recent progress in nitrogen-doped graphene: synthesis, characterization, and its potential applications, ACS Catal. 2 (2012) 781–794, https://doi.org/10.1021/cs200652y.
[20] Y. Wang, Y. Shao, D.W. Matson, J. Li, Y. Lin, Nitrogen-doped graphene and its application in electrochemical biosensing, ACS Nano 4 (2010) 1790–1798, https://doi.org/10.1021/nn100315s.
[21] M. Ghazinejad, S. Holmberg, O. Pilloni, L. Oropeza-Ramos, M. Madou, Graphitizing non-graphitizable carbons by stress-induced routes, Sci. Rep. 7 (2017) 16551, https://doi.org/10.1038/s41598-017-16424-z.
[22] B. Pollack, S. Holmberg, D. George, I. Tran, M. Madou, M. Ghazinejad, Nitrogen-rich polyacrylonitrile-based graphitic carbons for hydrogen peroxide sensing, Sensors 17 (2017) 2407, https://doi.org/10.3390/s17102407.
[23] I. Streeter, G.G. Wildgoose, L. Shao, R.G. Compton, Cyclic voltammetry on electrode surfaces covered with porous layers: an analysis of electron transfer kinetics at single-walled carbon nanotube modified electrodes, Sensor. Actuator. B Chem. 133 (2008) 462–466, https://doi.org/10.1016/j.snb.2008.03.015.
[24] K.K. Cline, M.T. McDermott, R.L. McCreery, others, Anomalously slow electron transfer at ordered graphite electrodes: influence of electronic factors and reactive sites, J. Phys. Chem. 98 (1994) 5314–5319.
[25] Q. Chen, G.M. Swain, Structural characterization, electrochemical reactivity, and response stability of hydrogenated glassy carbon electrodes, Langmuir 14 (1998) 7017–7026, https://doi.org/10.1021/la980907z.
[26] P. Chen, R.L. McCreery, Control of electron transfer kinetics at glassy carbon electrodes by specific surface modification, Anal. Chem. 68 (1996) 3958–3965.
[27] P.J.F. Harris, Fullerene-related structure of commercial glassy carbons, Philos. Mag. A 84 (2004) 3159–3167, https://doi.org/10.1080/14786430410001720363.
[28] P.J.F. Harris, Structure of non-graphitising carbons, Int. Mater. Rev. 42 (1997) 206–218.
[29] A.C. Ferrari, Raman spectroscopy of graphene and graphite: disorder, electron–phonon coupling, doping and nonadiabatic effects, Solid State Commun. 143 (2007) 47–57, https://doi.org/10.1016/j.ssc.2007.03.052.
[30] A. Sadezky, H. Muckenhuber, H. Grothe, R. Niessner, U. Pöschl, Raman microspectroscopy of soot and related carbonaceous materials: spectral analysis and structural information, Carbon 43 (2005) 1731–1742, https://doi.org/10.1016/j.carbon.2005.02.018.
[31] T. Xing, Y. Zheng, L.H. Li, B.C.C. Cowie, D. Gunzelmann, S.Z. Qiao, S. Huang, Y. Chen, Observation of active sites for oxygen reduction reaction on nitrogen-doped multilayer graphene, ACS Nano 8 (2014) 6856–6862, https://doi.org/10.1021/nn501506p.
[32] S.-M. Li, S.-Y. Yang, Y.-S. Wang, C.-H. Lien, H.-W. Tien, S.-T. Hsiao, W.-H. Liao, H.-P. Tsai, C.-L. Chang, C.-C.M. Ma, C.-C. Hu, Controllable synthesis of nitrogen-doped graphene and its effect on the simultaneous electrochemical determination of ascorbic acid, dopamine, and uric acid, Carbon 59 (2013) 418–429, https://doi.org/10.1016/j.carbon.2013.03.035.
[33] R.S. Nicholson, Theory and application of cyclic voltammetry for measurement of electrode reaction kinetics, Anal. Chem. 37 (1965) 1351–1355, https://doi.org/10.1021/ac60230a016.
[34] X. Ji, C.E. Banks, A. Crossley, R.G. Compton, Oxygenated edge plane sites slow the electron transfer of the ferro-/ferricyanide redox couple at graphite electrodes, ChemPhysChem 7 (2006) 1337–1344, https://doi.org/10.1002/cphc.200600098.
[35] J. Wang, T. Peng, Enhanced stability of glassy carbon detectors following a simple electrochemical pretreatment, Anal. Chem. 58 (1986) 1787–1790.
[36] M.L.A.V. Heien, P.E.M. Phillips, G.D. Stuber, A.T. Seipel, R. Mark Wightman, Overoxidation of carbon-fiber microelectrodes enhances dopamine adsorption and increases sensitivity, Analyst 128 (2003) 1413–1419, https://doi.org/10.1039/B307024G.
[37] J. Li, B.M. Christensen, Effect of pH on the oxidation pathway of dopamine and dopa, J. Electroanal. Chem. 375 (1994) 219–231, https://doi.org/10.1016/0022-0728(94)03389-7.
[38] C.D. Allred, R.L. McCreery, Adsorption of catechols on fractured glassy carbon electrode surfaces, Anal. Chem. 64 (1992) 444–448, https://doi.org/10.1021/ac00028a020.
[39] M. Megawati, C. Kiang Chua, Z. Sofer, K. Klímová, M. Pumera, Nitrogen-doped graphene: effect of graphite oxide precursors and nitrogen content on the electrochemical sensing properties, Phys. Chem. Chem. Phys. 19 (2017) 15914–15923, https://doi.org/10.1039/C7CP00520B.
[40] Z.-H. Sheng, X.-Q. Zheng, J.-Y. Xu, W.-J. Bao, F.-B. Wang, X.-H. Xia, Electrochemical sensor based on nitrogen doped graphene: simultaneous determination of ascorbic acid, dopamine and uric acid, Biosens. Bioelectron. 34 (2012) 125–131, https://doi.org/10.1016/j.bios.2012.01.030.
[41] K. Sudhakara Prasad, G. Muthuraman, J.-M. Zen, The role of oxygen functionalities and edge plane sites on screen-printed carbon electrodes for simultaneous determination of dopamine, uric acid and ascorbic acid, Electrochem. Commun. 10 (2008) 559–563, https://doi.org/10.1016/j.elecom.2008.01.033.
[42] M. Pumera, Electrochemistry of graphene, graphene oxide and other graphenoids: Review, Electrochem. Commun. 36 (2013) 14–18, https://doi.org/10.1016/j.elecom.2013.08.028.
[43] L. Tang, Y. Wang, Y. Li, H. Feng, J. Lu, J. Li, Preparation, structure, and electrochemical properties of reduced graphene sheet films, Adv. Funct. Mater. 19 (2009) 2782–2789, https://doi.org/10.1002/adfm.200900377.
[44] H. Wang, C. Zhang, Z. Liu, L. Wang, P. Han, H. Xu, K. Zhang, S. Dong, J. Yao, G. Cui, Nitrogen-doped graphene nanosheets with excellent lithium storage properties, J. Mater. Chem. 21 (2011) 5430–5434, https://doi.org/10.1039/C1JM00049G.
[45] C. Zhang, L. Fu, N. Liu, M. Liu, Y. Wang, Z. Liu, Synthesis of nitrogen-doped graphene using embedded carbon and nitrogen sources, Adv. Mater. 23 (2011) 1020–1024, https://doi.org/10.1002/adma.201004110.
[46] M. Sajid, M.K. Nazal, M. Mansha, A. Alsharaa, S.M.S. Jillani, C. Basheer, Chemically modified electrodes for electrochemical detection of dopamine in the presence of uric acid and ascorbic acid: a review, TrAC Trends Anal. Chem. 76 (2016) 15–29, https://doi.org/10.1016/j.trac.2015.09.006.
[47] N.G. Shang, P. Papakonstantinou, M. McMullan, M. Chu, A. Stamboulis, A. Potenza, S.S. Dhesi, H. Marchetto, Catalyst-free efficient growth, orientation and biosensing properties of multilayer graphene nanoflake films with sharp edge planes, Adv. Funct. Mater. 18 (2008) 3506–3514, https://doi.org/10.1002/adfm.200800951.
[48] P. Kissinger, W.R. Heineman, Laboratory Techniques in Electroanalytical Chemistry, second ed., CRC Press, 1996. Revised and Expanded.
[49] X. Mao, X. Yang, G.C. Rutledge, T. Alan Hatton, Ultra-wide-range electrochemical sensing using continuous electrospun carbon nanofibers with high densities of states, ACS Appl. Mater. Interfaces 6 (2014) 3394–3405, https://doi.org/10.1021/am405461j.